Time-dependent quantal calculations for $L=0$ models of the electron-impact ionization of hydrogen near threshold

F. Robicheaux, M. S. Pindzola, and D. R. Plante
Department of Physics, Auburn University, Auburn, Alabama 36849
(Received 22 October 1996)

The electron-impact ionization cross section for hydrogen near threshold is calculated using both time-dependent wave-packet and time-dependent Green's-function methods. The time-dependent Green's-function method also allows the calculation of the elastic cross section. The need for absorbing potentials was removed by allowing our fast waves to leave our two-dimensional grid. Two different models are used for the Coulomb interaction between the electrons: a cusp model with $v(r_1,r_2)=1/r_>$ and a linear model with $v(r_1,r_2)=1/(r_1+r_2)$, both with all angular momenta set to zero. Between 0.2 and 2.0 eV the cusp model cross section may exhibit an exponential suppression, while the linear model cross section follows a power-law behavior with an exponent of 1.1 with no noticeable oscillations. The results of the numerical experiments are compared with previous classical and quantal predictions extending back over 40 years to the pioneering work of Wannier. [S1050-2947(97)04305-9]

PACS number(s): 34.80.Dp, 34.10.+x

I. INTRODUCTION

The electron-impact ionization of hydrogen near threshold probes the correlated quantal dynamics of two slow electrons moving in the long-range Coulomb field of a third body. As such it remains one of the most fundamental unsolved problems in nonrelativistic quantum mechanics. The earliest classical dynamics analysis [1] derived a power-law dependence for the threshold ionization cross section in which the index was found to be equal to 1.127. Later, quantum theoretical analysis gave the same power-law dependence [2,3]. The fact that any analytic progress was made on this problem is striking because a complete quantal solution of the dynamics requires the solution of Schrödinger's equation in six space variables. The conservation of total angular momentum can be used to reduce the equation to three dynamical degrees of freedom which still constitutes a formidable theoretical problem. A full analytical solution is currently unknown for this particular three-body Schrödinger equation and only recently have numerical solutions been found at energies within 5 eV of threshold for electron ionization of hydrogen [4–6] and the related photodouble ionization of helium [7].

The threshold region for the escape of two electrons holds general interest because the form of the threshold law only depends on the asymptotic behavior of the potential and the symmetry of the wave function. The method used to initiate the simultaneous escape of two electrons of a certain symmetry only affects the overall size of the cross section without changing the energy dependence in the threshold region. These facts have allowed theoretical analysis of the threshold region with several quantum predictions for the dynamics; unfortunately, there is not complete agreement on the threshold law. The predictions are based on generic behavior of the potentials and wave functions and disagreement among the predictions casts serious doubt on our understanding of this fundamental process.

Before attacking the threshold laws for the full three-dimensional system, it seems wise to first carry out calculations for simpler model systems that have the same generic properties as the physical one. The model systems that we investigated are more amenable to numerical calculations than the full dynamics of two electrons near a heavy charged particle. The simplified models allow us to get converged results closer to threshold and test the difficulties in numerical threshold laws. As a bonus we are able to test the threshold laws obtained for the model systems [8–12]. This is an important intermediate step because the analytical methods that have been used on the model systems have also been applied to obtain threshold laws of physical systems.

The model systems we will investigate are simply a reduction of the full six-dimensional dynamics onto systems with only two degrees of freedom. These models restrict the angular momentum of each electron to be zero. The Schrödinger equation reduces to a partial differential equation in the radial coordinates of each electron. In the cusp model (or the Temkin-Poet model) [13,14] the exact electron interaction, $v(r_1,r_2)=1/|\mathbf{r}_1-\mathbf{r}_2|$, is replaced by $v(r_1,r_2)=1/r_>$, where $r_>$ is the larger of r_1 and r_2. This potential is simply the lowest term in the partial-wave expansion of the $1/r_{12}$ interaction. Although this potential is more directly related to the real potential it has some unfortunate features because of the cusp at $r_1=r_2$. In the linear model [15,16] the exact interaction is replaced by $v(r_1,r_2)=1/(r_1+r_2)$. This potential is motivated by the observation that the two electrons are on opposite sides of the nucleus for real two electron escape near threshold (i.e., $\mathbf{r}_1\simeq-\mathbf{r}_2$ which gives $|\mathbf{r}_1-\mathbf{r}_2| \simeq r_1+r_2$).

Recently there have been a number of time-independent methods [17–21] applied to electron-impact ionization in the cusp model. We choose, however, to investigate the threshold law using a time-dependent method [22–24]. One of the principal advantages of the latter method is that the time evolution of a wave packet does not require knowledge of the asymptotic form of the wave function. The wave-packet method is reviewed in Sec. II, a Green's-function method is presented in Sec. III, the ionization cross-section results for

the $L=0$ models are given in Sec. IV, and a brief summary is found in Sec. V. Atomic units are used throughout this paper except where otherwise noted.

II. TIME-DEPENDENT WAVE-PACKET METHOD

The time-dependent Schrödinger equation for these models is given by

$$i\frac{\partial\Psi(r_1,r_2,t)}{\partial t}=H(r_1,r_2)\Psi(r_1,r_2,t), \tag{1}$$

where the time-independent Hamiltonian is

$$H(r_1,r_2)=-\frac{1}{2}\frac{\partial^2}{\partial r_1^2}-\frac{1}{2}\frac{\partial^2}{\partial r_2^2}-\frac{Z}{r_1}-\frac{Z}{r_2}+v(r_1,r_2) \tag{2}$$

and $Z=1$. We solve this time-dependent equation using lattice techniques to obtain a discrete representation of the radial wave functions and all operators on a two-dimensional grid. The second derivatives with respect to r are approximated by a three-point second-order difference. No attempt is made to extract a bare ionization probability by deconvolution of the wave packet for fear of prejudice towards any particular form of the threshold law.

The total wave function at time $t=0$ is constructed as the symmetric product of an incoming radial wave packet for one electron and the lowest-energy bound stationary state of the other electron

$$\Psi(t=0)=\sqrt{\frac{1}{2}}\,[G_{ks}(r_1)P_{1s}(r_2)+P_{1s}(r_1)G_{ks}(r_2)], \tag{3}$$

where k is the linear momentum, $G_{ks}(r)$ is a radial wave packet, and $P_{1s}(r)$ is the ground-state radial orbital for hydrogen. Overall antisymmetrization is achieved by multiplying the radial wave function of Eq. (3) by a singlet spin function. We time evolve the partial differential equation using an explicit leap-frog propagator

$$\Psi(t+\Delta t)=\Psi(t-\Delta t)-2i\Delta t H\Psi(t), \tag{4}$$

where Δt is a small time step. The explicit time propagator can be more easily implemented on massively parallel computers than implicit methods. Further, relatively little information needs to be passed between processors because there is only one multiply by the Hamiltonian matrix. The leap-frog method has also found application in the time evolution of the Einstein equations describing black-hole collisions [25].

The total wave function at time $t=T$ following the collision is used to calculate the electron-impact ionization cross section given by

$$\sigma=\frac{\pi}{4k^2}(2S+1)\wp, \tag{5}$$

where by unitarity the probability of ionization is given by

$$\wp=1-2\sum_n\int dr_1\left|\int dr_2 P_{ns}(r_2)\Psi(r_1,r_2,t=T)\right|^2+\sum_m\sum_n\left|\int dr_1\int dr_2 P_{ms}(r_1)P_{ns}(r_2)\Psi(r_1,r_2,t=T)\right|^2. \tag{6}$$

This probability is calculated by finding the probability for finding *neither* electron in the negative-energy states of the grid. This is an approximation because the negative-energy states for large n are not physical states since they extend to a finite distance. Thus they have some continuum character. However, the positive-energy states on the grid have some bound-state character. By taking all of the unphysical negative-energy states and none of the unphysical positive-energy states in the projection, this gives the same results as projecting onto the physical negative-energy states to order inverse of box size squared.

There are several sources of error in the calculation. The first source of error arises in the approximate evaluation of the second derivatives in Eq. (2) using a grid of $\Delta r=0.2$ and in the discrete time propagation of Eq. (4) with $\Delta t=0.01$ These errors were negligible compared to other sources. A test calculation at 1 eV with $\Delta r=0.1$ and $\Delta t=0.0025$ gave the same answer as the coarser grid to within 0.2% as long as $\langle\Psi|H|\Psi\rangle$ was kept fixed for the different grids.

The finite size of the grid caused the largest errors for several reasons. The lattice size determines the spread in both coordinate and momentum space of the initial wave packet. The initial radial wave packet is given by

$$G_{ks}(r)=Ce^{-ikr}\exp\left[-\frac{(r-s)^4}{w^4}\right], \tag{7}$$

where C is a normalization constant. This form of the initial packet is chosen (as opposed to the usual Gaussian form) because the Fourier transform of this packet is more strongly peaked around k. Although it is not a minimum uncertainty packet, it achieves a tighter distribution in momentum space because the spatial extent of this packet is larger than for the Gaussian packet. If the maximum radius on the lattice is given by R, we choose the localization radius $s=R/2$ and the width parameter $w=R/4$. The full width at half maximum in momentum space is proportional to $1/w$. This is a main source of error in the calculation because the initial wave packet is made up of a distribution of energies. The final cross section is actually an infinite resolution cross section convolved over an energy $\Delta E=k\Delta k$. Since $k\simeq 1$ in our calculations, $\Delta E\simeq\Delta k$. For small ΔE, the error in the cross section will be proportional to ΔE^2 times the second derivative of the cross section with respect to energy.

In all of the calculations we made use of the fact that if one electron had a large group velocity the other electron was tightly bound. This fact allows the partition of the wave function into an inner region and an outer region as follows:

$$\Psi(r_1,r_2,t)$$
$$=\Psi(r_1,r_2,t), \quad 0<r_1<\frac{R}{2}, \quad 0<r_2<\frac{R}{2},$$
$$=\sum_n P_{ns}(r_1)\chi_{ns}(r_2,t), \quad 0<r_1<\frac{R}{2}, \quad \frac{R}{2}<r_2<R,$$
$$=\sum_n P_{ns}(r_2)\chi_{ns}(r_1,t), \quad \frac{R}{2}<r_1<R, \quad 0<r_2<\frac{R}{2}, \quad (8)$$

where $\Psi(r_1,r_2,t)$ satisfies Eqs. (1) and (2) in the inner region and $\chi_{ns}(r,t)$ satisfies

$$i\frac{\partial\chi_{ns}(r,t)}{\partial t}=\left(-\frac{1}{2}\frac{\partial^2}{\partial r^2}-\frac{(Z-1)}{r}+\epsilon_n\right)\chi_{ns}(r,t), \quad (9)$$

in the outer region. The sum over n in Eq. (8) includes the ground and lowest eigenstates, $P_{ns}(r)$, with corresponding eigenenergies ϵ_n. The outer region $\chi_{ns}(r,t)$ functions may be calculated quickly and have minimum storage requirements. The calculations are always stopped before the slow electrons (electrons attached to highly excited states or double-escape electrons) could reach the boundary between these regions. This partitioning of the wave function allows a cheap doubling of the accuracy of the calculation.

The finite grid size will give reflected waves from the $r=R$ boundary. The reflected waves can travel back to small r and scatter from the nucleus again. The fastest waves are those which have elastically scattered and thus have group velocity k. To prevent these waves from scattering from the core electron twice, the final time in our calculation is $T=3R/2k$. The elastic waves will have enough time to reflect from $r=R$ but not enough time to propagate back into the core region. Halting the time propagation at finite time introduces errors because the wave function has not evolved to its final form. This error is most pronounced at the lowest energies because the continuum waves are very slow near threshold. Obviously, increasing the lattice size reduces this error.

In Fig. 1 we present a contour plot for the $|\Psi|^2$ after the collision for the cusp model and Fig. 2 is the same except for the linear model. For both of these figures the energy is ~ 1 eV above the ionization threshold and the box extends to 200 a.u. The time for both figures is $t=R/k$. It is clear from these figures that the elastically scattered part of the wave travels much faster than any other part and is getting close to the wall at 200 a.u. The ionization part of the wave has hardly traveled at all, still being within ~ 75 a.u. of the nucleus. There is an interesting difference between the cusp model and linear model for the double continuum part of the wave, $r_1 \sim r_2$. In the cusp model electron probability has been pushed off of the line $r_1=r_2$ to some extent whereas the electron probability has a peak on the line $r_1=r_2$ for the linear model.

In Fig. 3 we plot the probability for both electrons to be in the continuum as a function of time for the 200 a.u. box at 1 eV above the ionization threshold. This plot is for the linear model. At small times, the electron has not yet scattered from the core so the probability is small. During the collision, the probability fluctuates because of the strong electron-electron interaction. At larger times, the probability approaches its asymptotic value.

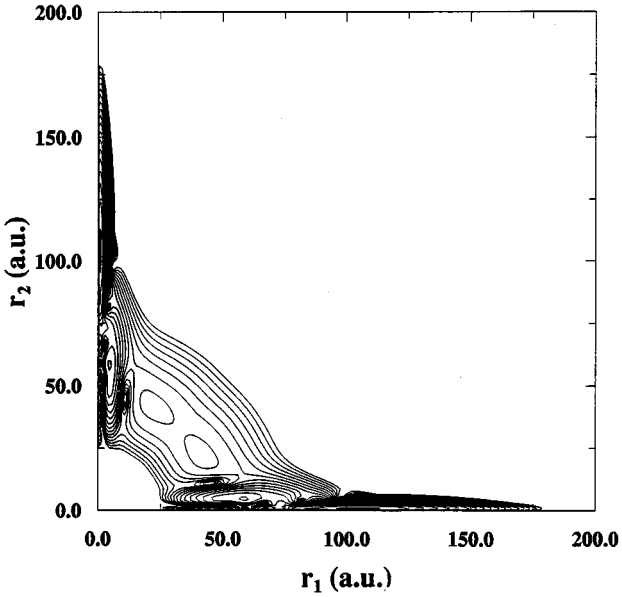

FIG. 1. Contour plot of the absolute value squared of the wave function 1 eV above the ionization threshold using the cusp model potential.

III. TIME-DEPENDENT GREEN'S-FUNCTION METHOD

In order to test the sources of error and perhaps provide a more accurate computational technique, we implemented a time-dependent Green's-function method. The derivation of this method in a formal and mathematically correct manner is fairly long and tedious. To circumvent this problem we give a heuristic derivation; the final results are the same but the journey is less tortured.

Any solution of the time-dependent Schrödinger equation

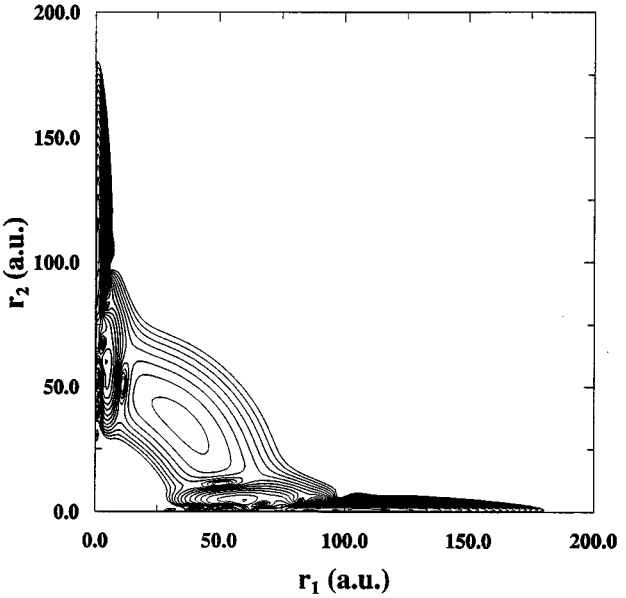

FIG. 2. Same as Fig. 1 but for the linear model potential.

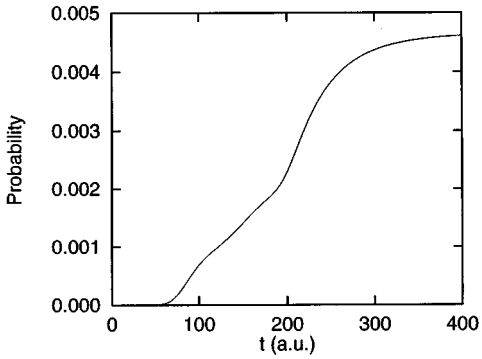

FIG. 3. Probability for both electrons to be in the continuum as a function of time for the 280 a.u. box at an energy 1 eV above the ionization threshold. The calculation is for the cusp model potential.

can be written as the superposition of two time-dependent functions,

$$\Psi(r_1,r_2,t)=\Lambda(r_1,r_2,t)+\Psi_0(r_1,r_2,t), \tag{10}$$

where

$$\Lambda(r_1,r_2,t)=\int dr_1'dr_2'dt' G(r_1-r_1',r_2-r_2',t-t') \times U(r_1',r_2',t')\Psi_0(r_1',r_2',t'), \tag{11}$$

with G being the exact Green's function for the full Hamiltonian. Alternatively, if the function $\Psi_0(r_1,r_2,t)$ is specified, then the function Λ is the solution of an inhomogeneous equation

$$\left[i\frac{\partial}{\partial t}-H(r_1,r_2)\right]\Lambda(r_1,r_2,t)=U(r_1,r_2,t)\Psi_0(r_1,r_2,t), \tag{12}$$

where the function $U(r_1,r_2,t)$ can be formally written as

$$U(r_1,r_2,t)\Psi_0(r_1,r_2,t)=\left[H(r_1,r_2)-i\frac{\partial}{\partial t}\right]\Psi_0(r_1,r_2,t). \tag{13}$$

These equations may be simply obtained by substituting the form for Ψ into Eq. (1). The inhomogeneous equation can be solved using the explicit leap-frog time propagator as is done for the wave-packet solution of the homogeneous equation.

Equation (12) is exact and has the same difficulties as Eq. (1); the interest in this split wave-function method is that it can serve as the basis of an approximate technique that at large times converges to an exact result. (We note that the full H acts on Λ; if we use $H-U$ to operate on Λ we recover first-order perturbation theory. By using the full H, we are not assuming any properties about U, for example, that U is small.) The $\Psi_0(r_1,r_2,t)$ function is chosen to be an energy eigenstate of a simple Hamiltonian which has one electron in the ground state and one electron in a continuum state

$$\Psi_0(r_1,r_2,t)=\sqrt{2/k}[\sin(kr_1)P_{1s}(r_2)+P_{1s}(r_1)\sin(kr_2)] \times\exp(-iEt), \tag{14}$$

where $E=\epsilon_{1s}+[1-\cos(k\Delta r)]/\Delta r^2$; this form for the energy is necessary when working near threshold because we must use the kinetic energy using the three-point difference. This choice for Ψ_0 gives an explicit form for U as

$$U(r_1,r_2,t)\Psi_0(r_1,r_2,t)=\sqrt{2/k}\left[\sin(kr_1)P_{1s}(r_2)\times\left\{-\frac{1}{r_1}+v(r_1,r_2)\right\}\right. \tag{15}$$

$$\left.+\sin(kr_2)P_{1s}(r_1)\times\left\{-\frac{1}{r_2}+v(r_1,r_2)\right\}\right]e^{-iEt}, \tag{16}$$

which is nonlocal but easily calculable on the grid. The Ψ_0 function is chosen so that there is one atomic unit of incoming flux (and one atomic unit of outgoing flux) in the continuum. Equation (12) is useless for calculations since the function U is always nonzero. However, we can use it for the base of our heuristic derivation.

The Green's-function method in this form does not work as well as the wave-packet method because the interaction is turned on instantaneously. The ''ringing'' this causes in Λ only very slowly decays with time. Suppose that the interaction potential U could be turned on slowly from zero to its correct asymptotic form given in Eq. (13). Then the inhomogeneous Schrödinger's equation would have the form

$$\left[i\frac{\partial}{\partial t}-H(r_1,r_2)\right]\Lambda(r_1,r_2,t)=F(t)U(r_1,r_2)\Psi_0(r_1,r_2,t), \tag{17}$$

where $F(t)$ is the turn on function. In our calculations we chose $F(t)=1/(1+\exp[10\{1-5t/t_f\}])$ with t_f the final time; this provides a smooth turn on for the inhomogeneous term. Because the interaction is turned on smoothly and slowly, the ringing in Λ is greatly reduced and the Green's-function method becomes more accurate than the wave-packet method.

Because Ψ_0 has unit incoming flux of electrons, the *rate* that electrons go into any channel in the Λ function equals the *probability* that an electron would have gone into that

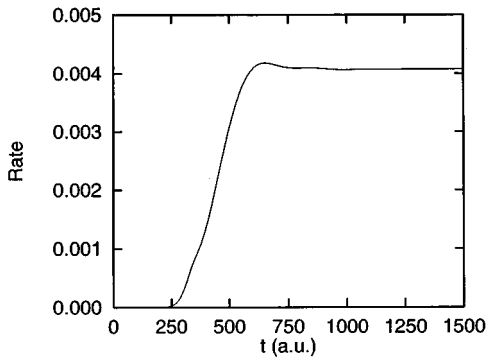

FIG. 4. Rate for both electrons to enter the continuum as a function of time for the 560 a.u. box at an energy 1 eV above threshold. The calculation is for the cusp model.

TABLE I. Electron-impact ionization cross sections (Mb) for hydrogen in the $L=0$ cusp model.

P (a.u.), E (eV)	$R=280$	$R=400$	$R=560$	$R=800$	$R=1000$
1.000, 0.088	0.0104	0.0055	0.0036	0.0019	0.0011
1.004, 0.196	0.0149	0.0092	0.0067	0.0047	0.0035
1.008, 0.305	0.0208	0.0145	0.0122	0.0095	
1.012, 0.414	0.0282	0.0216	0.0195	0.0165	
1.016, 0.524	0.0374	0.0307	0.0289	0.0256	
1.020, 0.634	0.0481	0.0417	0.0400	0.0367	
1.024, 0.744	0.0607	0.0547	0.0535	0.0497	
1.033, 0.995	0.0951	0.0899	0.0894		
1.041, 1.219	0.1319	0.1274	0.1278		
1.050, 1.473	0.1793	0.1754	0.1766		
1.066, 1.930	0.2752	0.2732	0.2761		

channel for an extremely wide wave packet; the *rate* that electrons go into a channel divided by the *rate* that electrons scatter from the core equals the probability for scattering into that channel. This method allows much longer time propagation and, hence, better energy resolution. For example, in our calculations the spread of energies in Λ is reduced by a factor of ~ 4 over that of the wave packets used in Eqs. (3) and (7) which reduces one of the main sources of error.

We monitored the rate that electrons entered the double continuum from $t=0$ to the final time. The rate that electrons entered the double continuum was obtained by calculating the amount of wave function in the double continuum as a function of time and numerically taking the time derivative. The amount of Λ in the double continuum is

$$A(t)=\langle\Lambda(t)|\Lambda(t)\rangle - 2\sum_n \int dr_1 \left| \int dr_2 P_{ns}(r_2)\Lambda(r_1,r_2,t)\right|^2 + \sum_{mn} |\langle P_{ns}P_{ms}|\Lambda(t)\rangle|^2. \quad (18)$$

Typically, we found that at short times the rate that electrons entered the double continuum was dominated by the rate that the inhomogeneous term was turned on with $F(t)$. The rate for entering the double continuum then slowly evolved to an asymptotic value. The speed that the asymptotic value is reached depends on the speed of the electrons in the double continuum; the asymptotic value was reached more quickly as the energy was increased. For some of the lower energies, the asymptotic value was not reached which was, of course, a major source of error.

In Fig. 4 we plot the rate to enter the double continuum for the cusp model at $E\sim 1$ eV above the ionization threshold using a 560 a.u. box. This plot shows how the rate approaches its asymptotic value and how the rate at short times is determined by the turn-on function, $F(t)$.

IV. CROSS-SECTION RESULTS

We performed a series of calculations for the $L=0$ model ionization cross sections, beginning with a 4.9×10^5 point lattice for $R=280$ and ending with a 6.25×10^6 point lattice for $R=1000$. The main bulk of the points cover the region $r_1, r_2 \leqslant R/2$ which is only 1/4 of the region covered by the wave function. We have solved Eq. (4) using several types of computers. For the smaller grids ($R\leqslant 560$), we utilized Sun work stations. For the $R=800$ runs, we used CRAY C90 supercomputers and Intel Paragon parallel computers. The $R=1000$ runs were carried out on the Paragons. To make use of massively parallel machines we divided the inner region wave function as follows:

$$\Psi_j(r_1,r_2,t)\neq 0 \quad \text{for } r_1<\frac{R}{2},\ \frac{(j-1)R}{2N}<r_2<\frac{jR}{2N}, \quad (19)$$

with each j strip on a separate processor and N total processors. For the wave-function partitions found in both Eqs. (8) and (19), the kinetic-energy operator requires message passing across the boundaries at $r=R/2$ and $r=jR/2N$, respectively. The discussion in this paragraph also applies to the inhomogeneous function, Λ.

The results of our calculations are presented in Tables I and II for the cusp model and Tables III and IV for the linear model. We would like to draw attention to several aspects of these tables: (1) the wave-packet method seems to have trouble converging the cusp model cross section with increasing box size, while the Green's-function method converges fairly rapidly. This is because the wave packet has a

TABLE II. Electron-impact ionization cross sections (Mb) for hydrogen in the $L=0$ cusp model with Green's function.

P (a.u.), E (eV)	$R=280$	$R=400$	$R=560$	$R=800$	$R=1000$
1.000, 0.088	0.000 20	0.000 12	0.000 11	0.000 09	0.000 11
1.004, 0.196	0.000 53	0.000 81	0.001 99	0.002 38	0.002 49
1.008, 0.305	0.002 89	0.005 32	0.007 60	0.006 70	
1.012, 0.414	0.0102	0.0135	0.0142	0.0133	
1.016, 0.524	0.0225	0.0213	0.0232	0.0223	
1.020, 0.634	0.0325	0.0330	0.0345	0.0334	
1.024, 0.744	0.0448	0.0449	0.0478	0.0464	
1.033, 0.995	0.0813	0.0819	0.0845	0.0823	
1.041, 1.219	0.1165	0.1191	0.1226		
1.050, 1.473	0.1635	0.1683	0.1719		
1.066, 1.930	0.2627	0.2660	0.2714		

TABLE III. Electron-impact ionization cross sections (Mb) for hydrogen in the $L=0$ linear model.

P (a.u.), E (eV)	$R=280$	$R=400$	$R=560$	$R=800$	$R=1000$
1.000, 0.088	0.0366	0.0317	0.0242	0.0185	0.0150
1.004, 0.196	0.0495	0.0414	0.0405	0.0360	0.0347
1.008, 0.305	0.0649	0.0630	0.0613	0.0592	
1.012, 0.414	0.0825	0.0798	0.0855	0.0855	
1.016, 0.524	0.1025	0.1057	0.1118	0.1128	
1.020, 0.634	0.1240	0.1283	0.1388	0.1400	
1.024, 0.744	0.1473	0.1553	0.1658	0.1668	
1.033, 0.995	0.2025	0.2136	0.2248		
1.041, 1.219	0.2525	0.2642	0.2752		
1.050, 1.473	0.3074	0.3187	0.3294		
1.066, 1.930	0.3981	0.4087	0.4186		

larger distribution of energies; as mentioned above, a distribution of energies gives a final cross section convolved over the energy distribution. (2) both the wave-packet and Green's-function method converge at roughly the same rate for the linear model. This is because the cross section for this case is roughly linear. (3) the lowest-energy point is *not* converged with either method for both models. However, the estimated errors are different for the different methods. We cannot estimate the ionization cross section for the cusp model at $E=0.088$ eV from the wave-packet method but we estimate that the ionization cross section from the Green's-function method is in the range $(1.1-2.2)\times10^{-4}$ Mb (from Table II it appears this cross section is converged, but the ionization rate was still increasing with time at the final time). Both the wave-packet and Green's-function method gives the cross section for the linear model to within 50% at the lowest energy. (4) the Green's-function method seems to give converged results (within 10%) down to 0.2 eV. (5) The prescription for achieving convergence, increased box size, seems to work.

In Fig. 5 we present the ionization cross section for the cusp model on a log-log graph. This graph is meant to highlight the strengths and/or weaknesses of the calculation as well as of two analytic methods. The dashed line is the

TABLE IV. Electron-impact ionization cross sections (Mb) for hydrogen in the $L=0$ linear model using Green's function.

P (a.u.), E (eV)	$R=280$	$R=400$	$R=560$	$R=800$	$R=1000$
1.000, 0.088	0.0020	0.0026	0.0058	0.0085	0.0112
1.004, 0.196	0.0109	0.0241	0.0346	0.0369	0.0383
1.008, 0.305	0.0445	0.0564	0.0649	0.0643	
1.012, 0.414	0.0756	0.0801	0.0920	0.0915	
1.016, 0.524	0.1003	0.1110	0.1195	0.1172	
1.020, 0.634	0.1288	0.1375	0.1467	0.1439	
1.024, 0.744	0.1607	0.1650	0.1732	0.1705	
1.033, 0.995	0.2129	0.2231	0.2318	0.2284	
1.041, 1.219	0.2699	0.2722	0.2795	0.2779	
1.050, 1.473	0.3227	0.3257	0.3329	0.3313	
1.066, 1.930	0.4080	0.4131	0.4208	0.4194	

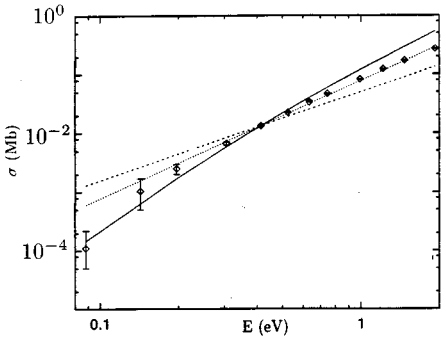

FIG. 5. Electron-impact ionization cross section for hydrogen in the $L=0$ cusp model. The dashed, dotted, and solid lines are from different analytic treatments discussed in the text.

power law $\sigma\propto E^{1.5}$ proposed in Ref. [8] and the solid line is the exponential form $\sigma\propto\exp(-6.87E^{-1/6}+4.00E^{1/6})$ proposed in Ref. [12]. The dotted line is the power law $\sigma\propto E^2$ which has no physical justification that we know of but seems to fit the energy dependence the best. It is clear that our results do not give the power-law dependence of Ref. [8]. It is possible that our results differ from power-law behavior near $E=0$ similar to the manner predicted in Ref. [12]. However, considering the problems with converging the lowest-energy point, we cannot unequivocably say whether or not we have good agreement.

In Fig. 6 we present the ionization cross section for the linear model on a log-log graph. The solid line is the power-law cross section $\sigma\propto E^{1.13}$ and the dashed and dotted lines correspond to $\sigma\propto E^{1.03}$ and $\sigma\propto E^{1.23}$. It is clear that our results give the expected $E^{1.13}$ power-law dependence very accurately, to better than 0.1 in the exponent since the 1.03 exponent does not rise fast enough while the 1.23 exponent rises too quickly. We have not done a least-squares fit to our data because we do not want to prejudice our results by choosing a particular form for the cross section, and because the low-energy points, where the threshold law will hold most accurately, are the least well known in our calculation. This graph is also informative in that we do not see the oscillations in the cross section predicted in Ref. [9] for $E>0.2$ eV. (Since our paper was submitted, Ref. [26] pre-

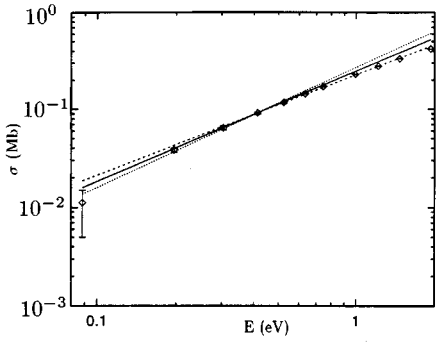

FIG. 6. Electron-impact ionization cross section for hydrogen in the $L=0$ linear model. The dashed, dotted, and solid lines are from different analytic treatments discussed in the text.

sented some results for the linear model in the threshold region.)

V. SUMMARY

We have shown that it is possible to obtain converged results into the threshold region ($E<2$ eV) for two continuum electrons in model problems. For these models, it appears that results are converged down to ~ 0.2 eV. The only parameter that was varied to give convergence is the size of the box containing the wave function. Estimates of convergence from these model calculations suggest that a full three-dimensional calculation could be made to converge down to ~ 1 eV and perhaps even lower. The finite difference method (or the finite element method) appears to be more amenable to attacking the threshold laws numerically than using basis function techniques. This is because the number of points goes like the size of the box squared. In basis function techniques, the number of basis functions also goes like the size of the box squared, but it is necessary to have the Hamiltonian between all of the basis functions, which means H goes like box size to the fourth power.

We showed that the time-dependent Green's-function technique was able to give convergence at least as fast as the more intuitive wave-packet method. This technique could also be utilized to calculate photodouble ionization cross sections near threshold. Both of the methods that we used took advantage of a staggered-leap-frog time propagation that is ideally suited for implementation on massively parallel machines. We found that by dividing the wave function into strips we were able to get linear speed up until the point that there were ~ 10 rows of points on each processor.

We were able to obtain results in the threshold region for the two models. This allowed us to distinguish between several proposals for the form of the threshold law. The only case that is still uncertain is for the exponential cutoff suggested for the cusp model. Of course, the conclusions in this paragraph are invalid if the threshold behavior is only in the region of energy less than 0.2 eV $\sim 1/100$ a.u.

ACKNOWLEDGMENTS

M.S.P. was supported in part by an NSF Grant (No. NSF-PHY-9122199) with Auburn University, F.R. was supported in part by an NSF Young Investigator Grant (No. NSF-PHY-9457903) with Auburn University, and D.R.P. was supported by a DOE EPSCoR grant. Computational work was carried out at the National Energy Research Supercomputer Center in Livermore, California, the Center for Computational Sciences in Oak Ridge, Tennessee, and the Alabama Supercomputer Center in Huntsville, Alabama.

[1] G. Wannier, Phys. Rev. **90**, 817 (1953).
[2] R. Peterkop, J. Phys. B **4**, 513 (1971).
[3] A.R.P. Rau, Phys. Rev. A **4**, 207 (1971).
[4] I. Bray and A. T. Stelbovics, Phys. Rev. Lett. **70**, 746 (1993).
[5] D. Kato and S. Watanabe, Phys. Rev. Lett. **74**, 2443 (1995).
[6] K. Bartschat and I. Bray, J. Phys. B **29**, L577 (1996).
[7] M. Pont and R. Shakeshaft, J. Phys. B **28**, L571 (1995).
[8] A. Temkin, Phys. Rev. Lett. **16**, 836 (1966).
[9] A. Temkin, Phys. Rev. Lett. **49**, 365 (1982).
[10] G. Handke, M. Draeger, W. Ihra, and H. Friedrich, Phys. Rev. A **48**, 3699 (1993).
[11] J. M. Rost, Phys. Rev. Lett. **72**, 1998 (1994).
[12] J. H. Macek and W. Ihra, Phys. Rev. A **55**, 2024 (1997).
[13] A. Temkin, Phys. Rev. **126**, 130 (1962).
[14] R. Poet, J. Phys. B **11**, 3081 (1978).
[15] R. Peterkop and L. Rabik, J. Phys. B **5**, 1823 (1972).
[16] A. Temkin and Y. Hahn, Phys. Rev. A **9**, 708 (1974).
[17] J. Callaway and D. H. Oza, Phys. Rev. A **29**, 2416 (1984).
[18] I. Bray and A. T. Stelbovics, Phys. Rev. Lett. **69**, 53 (1992).
[19] S. Watanabe, Y. Hosoda, and D. Kato, J. Phys. B **26**, L495 (1993).
[20] K. W. Meyer, C. H. Greene, and I. Bray, Phys. Rev. A **52**, 1334 (1995).
[21] K. Bartschat and I. Bray, Phys. Rev. A **54**, R1002 (1996).
[22] C. Bottcher, J. Phys. B **14**, L349 (1981).
[23] W. Ihra, M. Draeger, G. Handke, and H. Friedrich, Phys. Rev. A **52**, 3752 (1995).
[24] M. S. Pindzola and D. R. Schultz, Phys. Rev. A **53**, 1525 (1996).
[25] P. Anninos, K. Camarda, J. Masso, E. Seidel, W. Suen, and J. Towns, Phys. Rev. D **52**, 2059 (1995).
[26] D. Kato and S. Watanabe, J. Phys. B **29**, L779 (1996).